

VLBI Imagings of Kilo-parsec Knot in 3C 380

Shoko Koyama^{1,2}, Motoki Kino³, Hiroshi Nagai², Kazuhiro Hada⁴, Seiji Kamen⁵, and
Hideyuki Kobayashi^{1,2}

¹*Department of Astronomy, Graduate School of Science, The University of Tokyo, 7-3-1 Hongo,
Bunkyo-ku, Tokyo 113-0033, Japan*

shoko.koyama@nao.ac.jp

²*National Astromonomical Observatory of Japan, 2-21-1 Osawa, Mitaka, Tokyo 181-8588, Japan*

³*The Institute of Space and Astronautical Science, Japan Aerospace Exploration Agency, 3-1-1
Yoshinodai, Chuo-ku, Sagamihara, Kanagawa 252-5210, Japan*

⁴*INAF Istituto di Radioastronomia, via Gobetti 101, 40129 Bologna, Italy*

⁵*Department of Physics, Faculty of Science, Kagoshima University, 1-21-35 Korimoto, Kagoshima
890-0065, Japan*

(Received 2012 August 22; accepted 2012 October 19)

Abstract

We investigate observational properties of a kilo-parsec scale knot in radio-loud quasar 3C 380 by using two epoch archival data obtained by Very Long Baseline Interferometry (VLBI) at 5 GHz on 1998 July and 2001 April. We succeed in obtaining the highest spatial resolution image of the bright knot K1 located at 732 milliarcseconds, or ≥ 20 kpc de-projected, downstream from the nucleus three times better than previously obtained highest resolution image by Papageorgiou et al. (2006). Our images reveal, with new clarity, “inverted bow-shock” structure in K1 facing the nucleus and its morphology resembles a conical shock wave. By comparing the two epoch images directly, we explore the kinematics of K1 and obtain the upper limit of apparent velocity, 0.25 mas yr^{-1} or $9.8c$ of K1 for the first time. The upper limit of apparent velocity is marginally smaller than superluminal motions seen in the core region. Further new epoch VLBI observations are necessary to measure the proper motion at K1.

Key words: galaxies: active — galaxies: jets — galaxies: quasars: individual (3C 380 = 1828+487) — radio continuum: galaxies — techniques: interferometric

1. Introduction

Thanks to recent progress in the field of radio interferometry, the properties of knots at large scales (down to ~ 100 pc-10 kpc from the nucleus) in several nearby radio galaxies have

been investigated. For example, VLBI images clarify the detail complex internal structures such as knot HST-1 in M87 ($z = 0.0036$) (e.g., Cheung et al. 2007; Chang et al. 2010; Giroletti et al. 2012) and knot C80 in 3C 120 ($z = 0.033$) (e.g., Roca-Sogorb et al. 2010; Agudo et al. 2012), located 50-100 pc away from their nucleus (details and other examples are summarized in § 5.1.1). HST-1 complex, and knots D and E located at kpc order from the nucleus of M87, display superluminal motions up to $6c$ by Very Large Array (VLA), Hubble space telescope (HST) and VLBI (e.g., Biretta et al. 1995; Biretta et al. 1999; Cheung et al. 2007; Chang et al. 2010; Giroletti et al. 2012). The kinematics of knots in nearby broad line radio galaxy 3C 120 are also studied out to 3 kpc, but the none of the superluminal motion originally claimed by Walker et al. (1988) was found in further VLBI observations (Muxlow & Wilkinson 1991; Walker 1997).

As for radio-loud quasars, VLBI images at large scales, let alone their kinematics are hardly studied due to their locations and lack of spatial resolutions. Although the majority of the cores showing superluminal motions are quasars (e.g., Kellermann et al. 2004; Lister et al. 2009), it is not clear where jet deceleration happens. To develop a detailed understanding of the jet deceleration process and shock dissipation process at large scales, it is crucial to obtain direct images of kpc scale knots with sufficient spatial resolution. There is only one attempt to image kpc scale knots and constrain on their motions in radio-loud quasars. With a global VLBI network of 16 radio telescopes, Davis et al. (1991) conducted the observations of 3C 273 ($z = 0.158$) at 1.7 GHz. By comparing with an earlier image, they indicate a possible superluminal motion about $2-5c$ on 100 pc scales, but it is difficult to confirm because different components emerged.

To overcome the above shown difficulty and explore observational properties of large scale knots in radio-loud quasars, we select 3C 380 which is known as a compact steep spectrum (CSS) radio source ($z = 0.692$) with VLBI. As having a steep spectrum, this source is considered to be associated with a misaligned jet (Fanti et al. 1990). Since the position angle of each inner parsec scale jet, ranging from 284° to 352° , are almost parallel to their motion vectors, it is suggested that the jet was ejected ballistically from the core. There are two distant bright knots, K1 and K2, located ~ 0.73 and 1 arcseconds at position angle around 308° , which is approximately in the direction of continuation of the inner jet (Kameno et al. 2000). The distance between K1 and the core corresponds to more than 20 kpc, using viewing angle $\leq 15^\circ$ (e.g., Wilkinson et al. 1984; Kameno et al. 2000). Detection of the linear polarization by Multi-Element Radio Linked Interferometer Network (MERLIN) (Flatters 1987) and the optical emission by HST (deVries et al. 1997) at K1 and K2 implies the presence of strong interaction between the knots and ambient medium. K1 in 3C 380 is the best target to explore the observational properties of quasar kpc scale knot, because the knot is sufficiently bright and the source entire angular size is sufficiently compact for VLBI observations. We attempt to image the kpc scale knot K1 in 3C 380 with a high resolution VLBI.

The organization of this paper is as follows. The observation data and data reduction is described in § 2 and § 3, respectively. The results are presented in § 4 and the discussions are given in § 5. Throughout this paper, we adopt the following cosmological parameters : $H_0 = 71 \text{ km s}^{-1}\text{Mpc}^{-1}$, $\Omega_M = 0.27$, and $\Omega_\Lambda = 0.73$ (Komatsu et al. 2009), or $1 \text{ mas} = 7.11 \text{ pc}$ and $0.1 \text{ mas yr}^{-1} = 3.92c$.

2. Archival Radio Data

We analyzed two VLBI archival data of quasar 3C 380 at 4.815 GHz in left hand circular polarization, observations of which were made on 1998 July 4 and 2001 April 24. In Table 1, we summarize the details of the VLBI data. All the ten antennas of VLBA (Very Long Baseline Array) are used in the observations. The first epoch is our data as a part of VSOP (VLBI Space Observatory Programme) observation, including the Effelsberg telescope. The second epoch data is obtained from VLBA archival data services. All the correlation processes were performed by the National Radio Astronomy Observatory (NRAO) VLBA correlator in Socorro, NM, USA.

3. Data Reduction

We used the Astronomical Image Processing System (AIPS) software package developed by the NRAO for a priori amplitude calibration, fringe fitting, and passband calibration process. For the first epoch data, we did not use the data of spacecraft baselines. Since the distance between the core and K1 corresponds to around 700 beamwidth, time and frequency averaging would cause time and bandwidth smearing in the K1 region (Thompson et al. 2001). To minimize the smearing effect on K1 to make wide field of view images, the frequency channels were averaged within each IF, and these IFs were kept separate during imaging process. We did not use any time averaging, but the error on each visibility data point was also adopted as the standard deviation within ten seconds by using AIPS task FIXWT (see Table 1).

Imaging was performed using CLEAN and self-calibration algorithm. This was performed with the Difmap software package (Shepherd et al. 1994). We started imaging the core and the inner jet to eliminate the sidelobes from the core over K1, because we expected the K1 flux was around 10% of the integrated flux density of the inner jets, which was $\sim 2.0 \text{ Jy}$ at 5 GHz. We adopted both uniform and natural weighting, and performed phase-only self-calibration several times. After converging visibility phase model and observed phase, we imaged the inner jet and K1 together by applying natural weighting and uv -tapering and performed phase and amplitude self-calibration.

Since all the data had the shortest uv distance much longer than $143 \text{ k}\lambda$, which corresponded to half of the beam size $\sim 720 \text{ mas}$ which covered both core and K1 at 5 GHz, missing flux would be caused at K1. Therefore we only obtained the lower limit of the K1 flux.

4. Results

4.1. *Inverted Bow-shock Structure of K1*

In Fig. 1, we show the overall images of 3C 380 in total intensities. In the left panel, the entire image of 3C 380 and zoom-in core image are shown, while the K1 image is shown in the right panel with the beamsize of 1.66×1.10 mas resolution at beam position angle -32.5° . K1 in Fig. 1, located at around 0.73 arcsec away from the core, is detected with signal-to-noise ratio over eight. From Fig. 1, we find, with new clarity, the inverted bow-shock shaped structure in K1 edge-brightened region as is previously described (Simon et al. 1990; Wilkinson et al. 1991; Papageorgiou et al. 2006). This finding helps to confirm the original suggestion of inverted bow-shock structure in K1 by Cawthorne (2006) and Papageorgiou et al. (2006), with three times better resolution than these of their images. The width of K1 is about 280 pc (40 mas) measured perpendicular to the jet direction, which is the same size as the K1 diameter suggested by (Simon et al. 1990), and the length of K1 is 140 pc (20 mas) in our images. Compared with the previously obtained VLBI images of K1 (Fig. 12 in Papageorgiou et al. 2006; top left of Fig. 1 in Kameno et al. 2000), we have attained the highest spatial resolution image by adding outer five VLBA and Effelsberg telescopes. The spatial resolution of obtained K1 image is three times higher than that of the previously obtained highest resolution image of K1 at 1.6 GHz (the beam size of Fig. 12 in Papageorgiou et al. 2006 is 5.0×3.7 mas).

4.2. *Kinematics of K1*

We further attempt to explore the kinematics of K1 by comparing Gaussian-fitted peak positions of K1 in these two epoch images. In Fig. 2, we present the two epoch images of K1, using only VLBA ten antennas, with the common restored beam size 2.54×1.81 mas resolution at beam position angle -1.95° with natural weighting. From Fig. 2, we find that the inverted bow-shock structure seen in the first epoch image is also detected in the second epoch. This structure would be maintained between these two observations, that is, over 2.82 years.

To compare the position of K1 between 1998 July and 2001 April, we overlay two images of Fig. 2 to produce Fig. 3 left with reference to the core peak position measured by AIPS task JMFIT. Previous studies support that core brightness peak position converges to a stable point within 0.2 mas order (e.g., O’Sullivan & Gabuzda 2009; Hada et al. 2011). Since it is sufficiently small compared with our beam size, we can regard the core as stable in the present work. To measure the peak position and estimate the position accuracy of K1, we fit a single Gaussian model to each slice profile (Fig. 3 right) by using the task SLFIT in AIPS. From Fig. 3 right, we can find the core-facing edge of K1 in each epoch is located at the same position, that is, at ~ 725 mas distance from the core. The full width of half maximum (FWHM) of a single Gaussian fitted to slice profile of K1 is almost identical to the slight change of each image due to the method of self-calibration. The position accuracy of K1 is derived as a ratio of

FWHM of the fitted Gaussian to signal-to-noise ratio (SNR) at K1 (e.g., Walker 1997), which is conservatively estimated less than ~ 0.79 mas. The derived peak position and their accuracy is summarized in Table 3.

Finally we estimate the maximum apparent velocity of K1, $\beta_{\text{app,max}}$, as peak position displacement over $\Delta t = 2.82$ years with propagation of uncertainty. The peak position displacement is $\Delta R = R_1 - R_2 = -0.27$ mas, where R_1 and R_2 are the peak position at first epoch and second epoch, respectively. The error in the displacement is estimated to be 0.97 mas by using propagation of uncertainty, or the root-mean-square (r.m.s.) of the position uncertainty at each epoch. Therefore, the upper limit of the peak position displacement is $\Delta R_{\text{max}} = -0.27 + 0.97 = 0.70$ mas and the maximum apparent proper motion is estimated to be $\Delta R_{\text{max}}/\Delta t = 0.25$ mas yr $^{-1}$. Thus, we obtain $\beta_{\text{app,max}} = 9.8$.

5. Discussion

5.1. Internal Structures in Large Scale Knots/Hot Spots

5.1.1. Classification of previously known cases

As shown in the Introduction, VLBI observations of large-scale knots are quite limited and only a handful of sources are explored. Here, we classify them. Below, we attempt to categorize the internal structures into three typical ones. We do not include some known sources which are difficult to categorize because of their peculiarities (e.g., HST-1 in M87 by Giroletti et al. 2012; northern hot spot of broad line radio galaxy PKS 1421 – 490 by Godfrey et al. 2009).

Inverted bow-shock type— As shown in the previous section, the apex of K1 edge-brightened region in 3C 380 faces towards the core. In this work, we call this feature inverted bow-shock structure. The same structure as K1 in 3C 380 is found at C80 in 3C 120, which is the stationary jet feature located 140 pc (80 mas) away from the core with 35 pc in size (Agudo et al. 2012). The key common property between 3C 380 and 3C 120 is their viewing angle. They are classified as misaligned AGN (Abdo et al. 2010), since their viewing angles are larger than those of blazars but smaller than those of radio galaxies.

Bow-shock type— 3C 205 is known as a high-redshift quasar with large viewing angle because there exists a pair of strong hot spots. In the pioneer work of Lonsdale & Barthel (1998), VLBA images of the primary hot spot A in 3C 205 at 1.4 GHz are shown. The VLBI hot spot, located more than 40 kpc away from the core, has the overall size 1400 pc and the jet width around 250 pc. The apex of edge-bright region in hot spot A of 3C 205 against the core face the opposite direction of that of 3C 380. Therefore, here we call this feature bow-shock type structure to tell contrast to inverted bow-shock type. ¹

¹ Note that Lonsdale & Barthel (1998) focused on the asymmetry of bow-shock rather than the bow-shock and they discussed a bent-jet model which can explain the asymmetry.

Multi-spots type— There are several knots and spots having multi-spots in a hot spot. Pictor A is a representative of this. Tingay et al. (2008) reveals that the northwest hot spot in Pictor A at 3.5 kpc scale contains five compact pc-scale components in the spot. The sizes of these components are 30-170 pc. One of the other examples is the southern hot spot of FRI/FRII radio galaxy PKS 2153 – 69, which is 200 pc in diameter and contains three components as small as 50 pc Young et al. (2005). The hot spot is located 5 kpc away from the core and would trace the varying position of the precessing jet interaction region with clouds.

5.1.2. *Origin of various internal structures*

Bearing the above brief summary in mind, let us discuss possible origins of apparently different internal structures in large scale knots.

Viewing angle effect— The inverted bow-shock can be observed in broad-line radio galaxies (BLRGs) and CSS-QSOs, both of which have relatively narrow viewing angles. It is known that 3C 120 is identified as a BLRG and its viewing angle is estimated as $\theta \leq 19^\circ$ (e.g., Gómez et al. 2000) and CSS-QSO 3C 380 with inclination angle $\theta \leq 15^\circ$ (e.g., Wilkinson et al. 1984; Kameno et al. 2000). On the other hand, the viewing angle of quasar 3C 205 is suggested to be around 40° , which is the upper end of the quasar/radio galaxy unification according to low lobe flux density ratio (Bridle et al. 1994). Therefore, we speculate that the difference of viewing angles divide images into bow-shock and inverted bow-shock. This point has been already suggested by Cawthorne (2006), modeling the edge-bright region in K1 as a conical-shock seen with small viewing angle. Our work contributes to offer the highest resolution image of K1 structure with new clarity and to show the inverted bow-shock structure supporting the Cawthorne’s model.

Regarding the physical origin of bow-shock and inverted bow-shock, Lind & Blandford (1985) suggest that the bow-shock is caused by a fast stream moving at relativistic speed up the center of the jet, while for example, Norman et al. (1982) indicate the inverted bow-shock is triggered by Kelvin-Helmholtz instability inside the unshocked jet. In the case of K1 in 3C 380, the inverted bow-shock might be interpreted as the bent backflow (reverse shock) at the jet termination point (Mizuta et al. 2010), since (Wilkinson et al. 1991) mention that K1 is similar to a hot spot seen in the lobes of some Fanaroff-Riley class II sources seen approximately pole-on.

Precession effect— The jet precession effect, or we may say jet-jittering effect, is explored and modeled by Scheuer (1982) and Cox et al. (1991) and are known as the “dentist drill” model. We consider that when the direction of the straight jet changes, causing the termination point to vary over a large-scale spot larger than the cross section of the jet, dynamically young (or long-lived) relic components can be seen as multi-spots. The multi-spots seen in Pictor A can be explained by the dynamically young (or we may say the long-lived) relic components produced by the precessing jets (Tingay et al. 2008). They estimate that a typical synchrotron cooling time scale of these regions from 100 to 700 years is much longer than the dynamical (Alfvénic

crossing) time scale of a few decades and indicate that these are dynamically young regions.

5.2. Kinematics of kpc knot K1

First of all, we stress that the present work is the first attempt to constrain the upper limit on possible proper motion at kpc scales in radio-loud quasars. By comparing Gaussian peak position of K1 slice profiles in 1998 July and 2001 April as reference to the core peak position (§ 4.2), we constrain the resolution of K1 apparent proper motion up to 0.25 mas yr^{-1} , corresponding to apparent velocity $\beta_{\text{app,max}} = 9.8$. In the core region, proper motions of several components are measured by Kameno et al. (2000) and Lister et al. (2009), ranging from $1.2c$ to $15c$, from sub-mas to 30 mas away from the core, respectively. Our constraint is marginally slower than the fastest and outermost apparent motions measured in the core region, which is the apparent motion of component F, 0.38 mas yr^{-1} or $15c$, labeled by Kameno et al. (2000)². This implies the jet deceleration or bending occurs between inner jet and K1, or the ejection angle (viewing angle) of K1 has changed from those of the inner jets assuming straight ballistic jets. To confirm jet proper motion at large scales with the maximum resolution of apparent velocity less than $2c$, further new epoch VLBI observation more than 14 years interval from the first epoch observation is required. In the case of jet bending, the apparent position angle difference $\phi_{\text{pos}} \sim 13^\circ$ between F and K1 would be magnified by projection with fixed small viewing angle ($\theta_{\text{view}} \leq 15^\circ$). Intrinsic jet bending angle ϕ_{bend} is estimated to be $\leq 3.3^\circ$, where $\tan \phi_{\text{bend}} = \tan \phi_{\text{pos}} \times \sin \theta_{\text{view}}$ (Kameno et al. 2000). As for the changes of jet ejection angle, if we assume the same intrinsic velocity $\beta = 0.9978$ for F and K1, the viewing angle should be 3.8° for component F and 1.4° or 10.2° for K1.

5.3. Future prospect

As a first step, we deal with only 5 GHz VLBI data in this paper. Here we mention future prospects to investigate the properties of K1.

5.3.1. Low frequency spectrum turnover

Low frequency spectrum turnover can constrain the jet component properties such as magnetic field strength (e.g., PKS 1421 – 490: Godfrey et al. 2009). Regarding the case of K1 in 3C 380, previous work of Megn et al. (2006) suggests spectral flattening below $\sim 100 \text{ MHz}$. However discussions in Megn et al. (2006) are based on flux values collected from literatures derived from various different interferometers and in which K1 is smaller than the beam size of each interferometer. Therefore, it seems difficult to determine fluxes accurately. Square Kilometer Array (SKA)³ will, in future, tell us the real turnover frequency with sufficiently high resolution.

² Values are recalculated with the cosmology parameters shown in § 1

³ <http://www.skatelescope.org/>

5.3.2. Polarization properties

Polarization properties are crucial to explore magnetic field geometries. Only Papageorgiou et al. (2006) report the resolved distribution of magnetic vector polarization angle (MVPA) in K1. The MVPA distribution appears tangential to the inverted bow-shock. In order to clarify a change of shock structure in K1, time-variation of MVPA is one of the key quantities for future observations because the sudden change of MVPA strongly suggest the existence of magnetohydrodynamical fast/slow mode waves (e.g., Nakamura et al. 2011). To clarify polarization properties of synchrotron emission is also substantial (Nalewajko & Sikora 2012) for testing reconfinement shock models (e.g., Komissarov & Falle 1997; Stawarz et al. 2006; Bromberg & Levinson 2009).

6. Summary

To explore the properties of kpc scale knots in radio-loud quasars, we produced the pc scale images of distant knot K1 in a bright CSS quasar 3C 380 with VLBI. Below we summarize the main results obtained in this work.

1. Using VLBA plus Effelsberg telescopes at 5 GHz with the technique of wide field imaging, we succeed in obtaining the highest resolution images of the pc scale structure of K1, located at more than 20 kpc downstream of the core. We confirm the edge-brightened region in K1 on the side of facing the core as the inverted bow-shock, which is the clear indication of conical shock with misaligned viewing angle.
2. Comparing VLBA ten antennas images of K1 in 1998 July and 2001 April referencing to the core brightness peak, the edge-brightened regions are located at ~ 725 mas. We constrain the upper limit on the possible proper motion of K1 up to 0.25 mas yr^{-1} or $9.8c$. Since our constraint on the apparent velocity is marginally slower than the fastest knot apparent motions of the core region, jet deceleration, bending, or precession could have occurred. Further new epoch VLBI observation is needed to confirm the proper motion of K1 with the resolution of apparent velocity $\leq 2c$.

We are grateful to K. Asada and A. Doi for constructive discussions. We thank the anonymous referee for useful comments and suggestions. S.K. acknowledges this research grant provided by the Global COE program of University of Tokyo. This work was partially supported by Grant-in-Aid for Scientific Researches, KAKENHI 2450240 (MK) from the Japan Society for the Promotion of Science (JSPS). This research has made use of data from National Radio Astronomy Observatory (NRAO) archive. The NRAO is a facility of the National Science Foundation operated under cooperative agreement by Associated Universities, Inc.

References

- Abdo, A. A., Ackermann, M., Ajello, M., et al. 2010, *ApJ*, 720, 912
- Agudo, I., Gómez, J. L., Casadio, C., Cawthorne, T. V., & Roca-Sogorb, M. 2012, *ApJ*, 752, 92
- Biretta, J. A., Zhou, F., & Owen, F. N. 1995, *ApJ*, 447, 582
- Biretta, J. A., Sparks, W. B., & Macchetto, F. 1999, *ApJ*, 520, 621
- Bridle, A. H., Hough, D. H., Lonsdale, C. J., Burns, J. O., & Laing, R. A. 1994, *AJ*, 108, 766
- Bromberg, O., & Levinson, A. 2009, *ApJ*, 699, 1274
- Cawthorne, T. V. 2006, *MNRAS*, 367, 851
- Chang, C. S., Ros, E., Kovalev, Y. Y., & Lister, M. L. 2010, *A&A*, 515, A38
- Cheung, C. C., Harris, D. E., & Stawarz, L. 2007, *ApJL*, 663, L65
- Cox, C. I., Gull, S. F., & Scheuer, P. A. G. 1991, *MNRAS*, 252, 558
- Davis, R. J., Muxlow, T. W. B., & Unwin, S. C. 1991, *Nature*, 354, 374
- de Vries, W. H., O’Dea, C. P., Baum, S. A., et al. 1997, *ApJS*, 110, 191
- Fanti, R., Fanti, C., Schilizzi, R. T., et al. 1990, *A&A*, 231, 333
- Flatters, C. 1987, *Nature*, 326, 683
- Gioletti, M., Hada, K., Giovannini, G., et al. 2012, *A&A*, 538, L10
- Godfrey, L. E. H., Bicknell, G. V., Lovell, J. E. J., et al. 2009, *ApJ*, 695, 707
- Gómez, J.-L., Marscher, A. P., Alberdi, A., Jorstad, S. G., & García-Miró, C. 2000, *Science*, 289, 2317
- Hada, K., Doi, A., Kino, M., et al. 2011, *Nature*, 477, 185
- Kameno, S., Inoue, M., Fujisawa, K., Shen, Z.-Q., & Wajima, K. 2000, *PASJ*, 52, 1045
- Kellermann, K. I., Lister, M. L., Homan, D. C., et al. 2004, *ApJ*, 609, 539
- Komatsu, E., Dunkley, J., Nolta, M. R., et al. 2009, *ApJS*, 180, 330
- Komissarov, S. S., & Falle, S. A. E. G. 1997, *MNRAS*, 288, 833
- Lind, K. R., & Blandford, R. D. 1985, *ApJ*, 295, 358
- Lister, M. L., Cohen, M. H., Homan, D. C., et al. 2009, *AJ*, 138, 1874
- Lonsdale, C. J., & Barthel, P. D. 1998, *AJ*, 115, 895
- Megn, A. V., Rashkovskii, S. L., Shepelev, V. A., et al. 2006, *Astronomy Reports*, 50, 692
- Mizuta, A., Kino, M., & Nagakura, H. 2010, *ApJL*, 709, L83
- Muxlow, T. W. B., & Wilkinson, P. N. 1991, *MNRAS*, 251, 54
- Nakamura, M., Meier, D. L., & Garofalo, D. 2011, *Ap&SS*, 336, 15
- Nalewajko, K., & Sikora, M. 2012, *A&A*, 543, A115
- Norman, M. L., Winkler, K.-H. A., Smarr, L., & Smith, M. D. 1982, *A&A*, 113, 285
- O’Dea, C. P., de Vries, W., Biretta, J. A., & Baum, S. A. 1999, *AJ*, 117, 1143
- O’Sullivan, S. P., & Gabuzda, D. C. 2009, *MNRAS*, 400, 26
- Papageorgiou, A., Cawthorne, T. V., Stirling, A., Gabuzda, D., & Polatidis, A. G. 2006, *MNRAS*, 373, 449
- Roca-Sogorb, M., Gómez, J. L., Agudo, I., Marscher, A. P., & Jorstad, S. G. 2010, *ApJL*, 712, L160
- Scheuer, P. A. G. 1982, *Extragalactic Radio Sources*, 97, 163
- Shepherd, M. C., Pearson, T. J., & Taylor, G. B. 1994, *BAAS*, 26, 987
- Simon, R. S., Readhead, A. C. S., Moffet, A. T., et al. 1990, *ApJ*, 354, 140
- Stawarz, L., Aharonian, F., Kataoka, J., et al. 2006, *MNRAS*, 370, 981

- Thompson, A. R., Moran, J. M., & Swenson, G. W., Jr. 2001, *Interferometry and synthesis in radio astronomy*. 2nd ed. New York : Wiley, p. 119-208
- Tingay, S. J., Lenc, E., Brunetti, G., & Bondi, M. 2008, *AJ*, 136, 2473
- Walker, R. C., Walker, M. A., & Benson, J. M. 1988, *ApJ*, 335, 668
- Walker, R. C. 1997, *ApJ*, 488, 675
- Wilkinson, P. N., Booth, R. S., Cornwell, T. J., & Clark, R. R. 1984, *Nature*, 308, 619
- Wilkinson, P. N., Akujor, C. E., Cornwell, T. J., & Saikia, D. J. 1991, *MNRAS*, 248, 86
- Young, A. J., Wilson, A. S., Tingay, S. J., & Heinz, S. 2005, *ApJ*, 622, 830

Table 1. Details of the VLBI observations at 4.815 GHz

Date	code	t_{on}^* [min]	Antennas [†]	BW [‡] [MHz]	Channels [§]		t_{acc}^l [sec]
					no.	sep. [kHz]	
1998/Jul/04	V125	770	VLBA10, EB	16	32	500	4
2001/Apr/24	W410	619	VLBA10	16	128	125	4

* Total on source time.

† Antennas : VLBA 10=Pie town NM USA, Los Alamos NM USA, Fort Davis TX USA, Owens Vally CA USA, Kitt Peak AZ USA, North Liberty IA USA, Hancock NH USA, Brewster WA USA, Saint Croix VI USA, Mauna Kea HI USA, EB : Effelsberg Germany.

‡ Total bandwidth.

§ Channel numbers per 1 IF and channel width per 1 channel.

^l Data accumulation period.

Table 2. Image performances of Fig. 2 with VLBA ten antennas

Date	Synthesized beam			S_{tot}^\dagger [Jy]	S_{peak}^\ddagger [mJy beam ⁻¹]	r.m.s. [§] [mJy beam ⁻¹]
	a_{maj}	a_{min}	P.A.			
	[mas]	[mas]	[°]			
1998/Jul/04	2.37	1.97	-12.1	2.30	835	0.139
2001/Apr/24	2.54	1.81	-1.95	2.12	934	0.172

* Long axis, short axis, and position angle of synthesized beam.

† Total cleaned flux of entire image.

‡ Peak flux of the entire image.

§ Root-mean-square noise of entire map.

Table 3. Properties of K1 in Fig. 2

Date	S_{K1}^* [mJy]	$S_{K1,peak}^\dagger$ [mJy beam $^{-1}$]	SNR_{K1}^\ddagger	FWHM § [mas]	Peak position l [mas]
1998/Jul/04	≥ 152	≥ 2.60	≥ 18.7	10.42	732.53 ± 0.56
2001/Apr/24	≥ 163	≥ 2.41	≥ 14.0	11.09	732.26 ± 0.79

* Integrated flux of K1 by using AIPS task IMSTAT.

† Peak flux of K1 derived from the Gaussian model fitted to each slice profile by using AIPS task SLICE and SLFIT.

‡ SNR of K1, or peak flux divided by r.m.s. noise in Table 2. The residual after fitting Gaussian to each slice profile is as small as the r.m.s. noise of the entire map.

§ FWHM of Gaussian model fitted to K1 slice profile using SLFIT.

l K1 peak position measured by SLFIT. The reference position is core brightness peak. The position error is FWHM over SNR of K1.

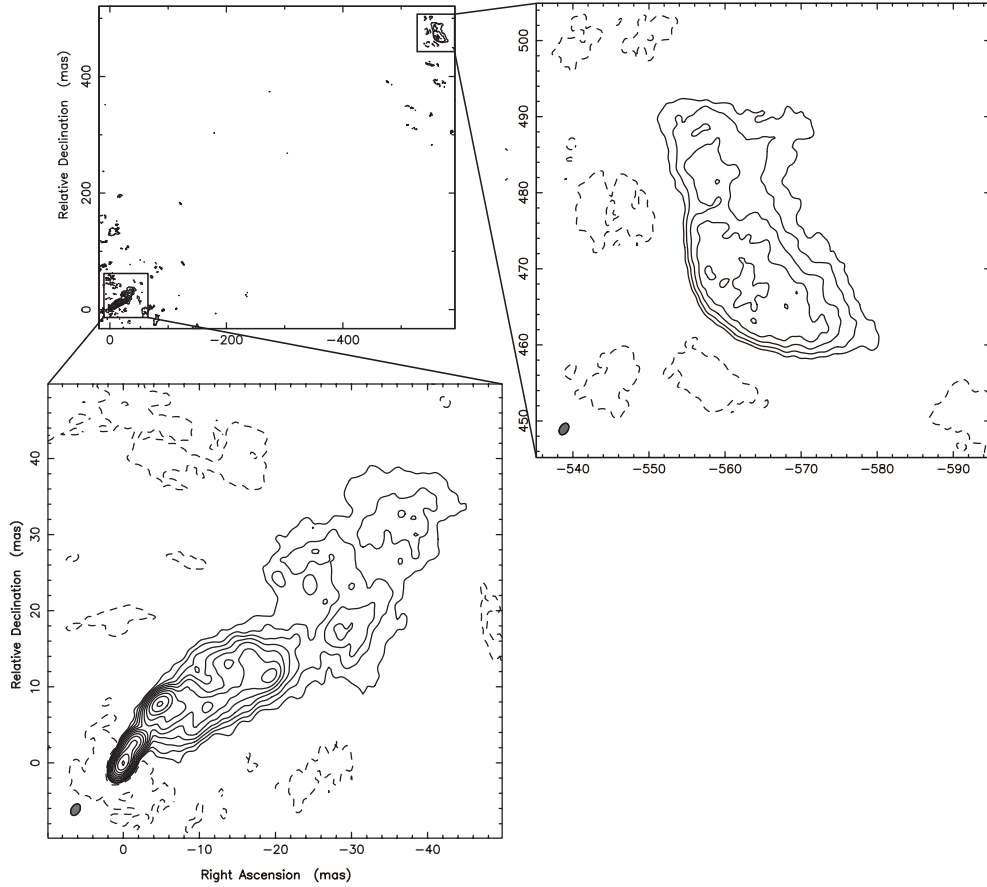


Fig. 1. Top left panel shows 3C 380 entire image obtained by VLBA ten antennas plus Effelsberg telescope on 1998 July 4 at 4.815 GHz with a resolution of $1.66 \text{ mas} \times 1.10 \text{ mas}$ in $\text{P.A.} = -32.5^\circ$, which is shown at bottom left corner of each image. The bottom-left panel displays the zoom-in image around the core with contour levels $0.328 \times (-1, 1, 1.41, 2, 2.83, 4) \text{ mJy beam}^{-1}$. The right panel shows the zoom-in image at K1 with contour levels $0.328 \times (-1, 1, 2, 4, 8, \dots, 2056) \text{ mJy beam}^{-1}$. Each lowest contour is 3σ level. Natural weighting is applied.

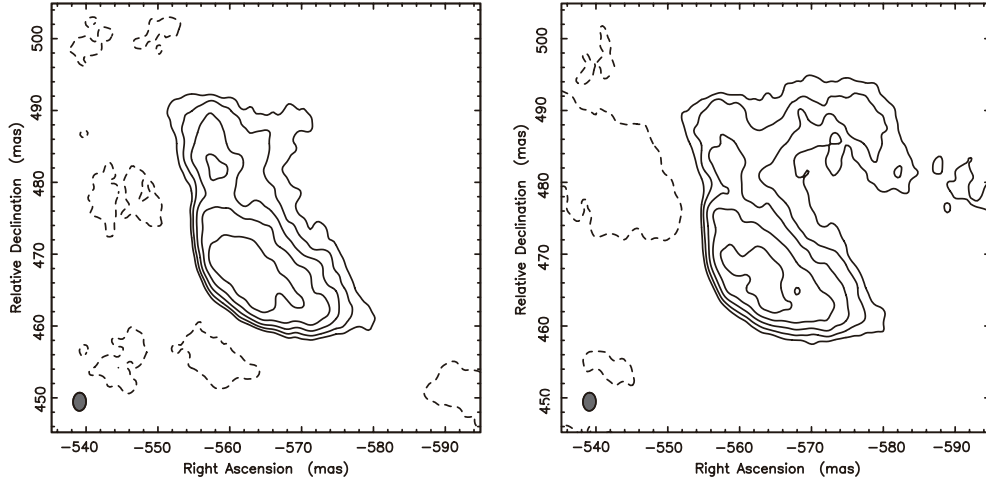


Fig. 2. Natural weighted images of K1 at 4.815 GHz with VLBA ten antennas. Left image data is obtained on 1998 July 4 and right image data is on 2001 April 24. All beam sizes are restored to $2.54 \text{ mas} \times 1.81 \text{ mas}$ in $\text{P.A.} = -1.95^\circ$, which is the original resolution of the right map. Contour levels are $0.765 \times (-1, 1.4142, 2, 2.83, 4) \text{ mJy beam}^{-1}$, which are aligned to the higher 3σ level (2001 data). The details of these two images are summarized in Tables 2 and 3.

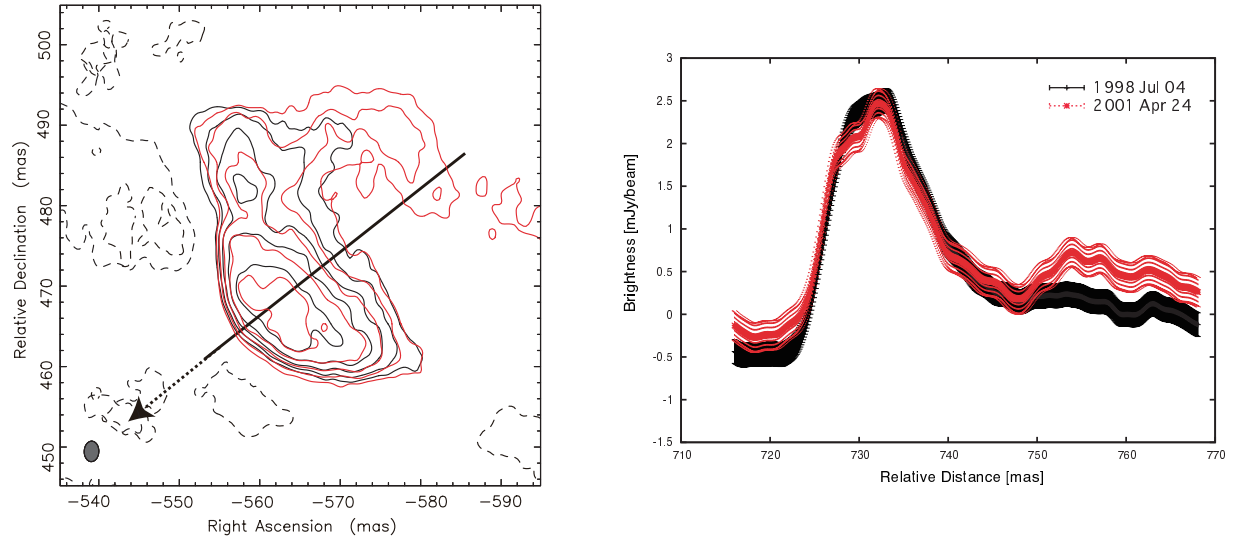


Fig. 3. Left image is 1998 July 4 image overlaid by 2001 April 24 image shown in Fig. 2 with reference to the core brightest peak. The straight line shows the slice position. The slice position is determined along the line connecting the core peak position and mean K1 peak position measured by AIPS task MAXFIT. The dotted arrow indicates the direction to the nucleus. Right image shows the slice profiles of K1, along the straight line shown in the left image. We put 1σ flux error (or image r.m.s. noise in Table 2) on each data point.